Colloids and Surfaces B: Biointerfaces 157 (2017) 31–39

Contents lists available at ScienceDirect

Colloids and Surfaces B: Biointerfaces

journal homepage: www.elsevier.com/locate/colsurfb

Quick and sensitive SPR detection of prion disease-associated isoform (PrP^{Sc}) based on its self-assembling behavior on bare gold film and specific interactions with aptamer-graphene oxide (AGO)

Zhichao Lou[a,b,*], Jinfeng Wan[a], Xiaohong Zhang[c], Haiqian Zhang[c], Xiaoyan Zhou[a], Su Cheng[d], Ning Gu[b]

[a] College of Materials Science and Engineering, Nanjing Forestry University, Nanjing 210037, China
[b] State Key Laboratory of Bioelectronics, Jiangsu Key Laboratory for Biomaterials and Devices, School of Biological Science and Medical Engineering, Southeast University, Nanjing 210096, China
[c] College of Materials Science and Technology, Nanjing University of Aeronautics and Astronautics, Nanjing 210016, China
[d] Zhongda Hospital, Southeast University, Nanjing 210009, China

ARTICLE INFO

Article history:
Received 6 March 2017
Received in revised form 18 April 2017
Accepted 23 May 2017
Available online 25 May 2017

Keywords:
Surface plasmon resonance
Prion protein
Aptamer-graphene oxid
Sandwich
Self-assembling

ABSTRACT

Herein, we constructed a novel sandwich surface plasmon resonance (SPR) detection assay for sensitive prion disease-associated isoform (PrP^{Sc}) detection, utilizing bare gold film and apatamer-graphene oxide (AGO). Due to the self-assembling behavior of PrP^{Sc} on gold surface, the non-modified gold surface can be directly used as sensing surface for the quick detection, for the purpose to avoid the interference from the traditional, complex and changeable probe-modified sensing surface. And due to the highly specific affinity of AGO towards PrP^{Sc}, the sandwich type SPR sensor exhibits excellent analytical performance towards the discrimination and quantitation of PrP^{Sc}. A good linear relationship was obtained between SPR responses and the logarithm of PrP^{Sc} concentrations over a range of 0.001–1 ng/mL. The detection sensitivity for PrP^{Sc} was improved by ~156 orders of AGO compared with SPR direct detection format. Besides, morphological changes of the sensing film surfaces were investigated by high resolution AFM imaging, confirming the capture of PrP^{Sc} molecules and their further specific recognition by AGO. The specificity of the present biosensor was also investigated by PrP^{C} and other regents as controls. By compared with other reported methods, the AGO enhanced sandwich SPR assay was confirmed to be efficient, sensitive, and with wide working range.

1. Introduction

Prion diseases are recognized as highly contagious and scarcely incurable, and are of a worldwide great concern [1–3]. Prion protein has drawn great attention due to its pathological potential to prion diseases [4]. PrP^{C} and PrP^{Sc} are two isoforms with the same amino acid sequence, but are different in conformation. PrP^{Sc} is supposed to be a marker for transmissible spongiform encephalopathies infections, and is also considered to be the causative agent [5,6]. In certain conditions, β-sheet rich PrP^{Sc} can introduce the transformation of PrP^{C} into PrP^{Sc} [7,8]. By now, the pathological concentration of PrP^{Sc} in human beings is unknown, but the minimum lethal dose in hamsters is reported less than 2 nM [9]. Thus, discriminate and detection of the trace quantities of PrP^{Sc} is an important measure for prion disease diagnosis at the presymptomatic stage.

In decades, numerous traditional methods have been proposed to detect PrP^{Sc}, such as protein misfolding cyclic amplification (PMCA) [10,11], ELISA [12], micromechanical resonator arrays [13,14], fluorescence correlation spectroscopy [15], FIAsH fluorescence [16], and immune-quantitative real-time PCR assays [17]. These assays have been proved to be sensitive, fledged and commonly-used in practical tests. But they are not suitable for the use of high-throughput detection or routine testing because they require practiced experimental skills and expensive instrumentations, and they are time- and labor-consuming. Nowadays, surface plasmon resonance (SPR) sensors are fully commercialized tools for quantifying various molecules involving in theranostics, pharmaceutics, food safety, environmental monitoring, and homeland security [18–20]. With the revolutionary developments of nanoscience, many scientific reports suggest that a lower limit of detection and a wider detection range can be obtained when

* Corresponding author at: College of Materials Science and Engineering, Nanjing Forestry University, Nanjing 210037, China.
E-mail address: zc-lou2015@njfu.edu.cn (Z. Lou).

http://dx.doi.org/10.1016/j.colsurfb.2017.05.058
0927-7765/

integrating nanomaterials into a miniaturized SPR system [21–23]. However, nanomaterials-enhanced SPR-based detection methods for the detection of PrP^{Sc} are barely reported [24,25].

Current SPR systems are involved in initial receptor immobilization onto the SPR gold film, to establish a specific sensing film. But this perspective is time-consuming, and needs to be re-considered. Our previous work suggests that these processes result in a rough sensing surface with various conformations of the receptor on it, causing unavoidable non-specific interactions at the nano-bio interfaces at single-molecule level. These interactions are supposed to affect the specificity of the SPR detection system [26]. Actually, bare gold films have been used in electrochemical [27,28] and SPR [29–31] detections of various molecules, considering their convenient surface treatment requirements and in-complex surface topographies. PrP^{Sc} molecules (monomers, dimers and trimers, Fig. S1B, the corresponding molecular dynamic simulation was described in details in the Supporting Information) are proved to self-assemble on gold surface via a coupling reaction between the disulfide bond and gold atoms [32,33]. This kind of self-assembly of proteins on inorganic substrates is now of great interest for biomedical engineering, providing a novel approach to the development of SPR [34,35]. William James and co-workers optimize and select a RNA aptamer (SAF-93), which binds selectively to PrP^{Sc}, and can be used in the detection of PrP^{Sc} in vitro [36,37]. From the three-dimensional structures of PrP^{Sc} molecules in Fig. S1B, we can confirm that the active sites in PrP^{Sc} towards SAF-93 remain free and available to SAF-93 when PrP^{Sc} molecules self-assemble on the gold surface.

Herein, we constructed a novel sandwich SPR detection assay for sensitive PrP^{Sc} detection (Fig. 1). Our results confirmed that the non-modified gold surface could be directly used as sensing surface for the quick detection due to the self-assembling behavior of PrP^{Sc} on gold surface. AGO sheets were used as recognition and amplification reagents for the enhancement of SPR signals. This sandwich type SPR sensor here exhibited excellent analytical performance towards the quantification and quantitation of PrP^{Sc}, with high sensitivity and good selectivity. Atomic force microscope (AFM) was used to investigate the morphology of the SPR substrate surface after the detection. To the best of our knowledge, it was the first time that PrP^{Sc} was detected by means of SPR with bare gold film as sensing film and with AGO as signal enhancement regent. This proposed approach can also be used to detect other analytes with similar thiol groups by altering the corresponding aptamer in the AGO conjugates.

2. Experimental methods

2.1. Chemicals

Prion protein was purchased from Calbiochem® in Germany (sequence: aa 23-231, shown in Fig. S1A, theoretical PI/Mw: 9.39/23571.92). PBS (pH 7.2) was purchased from Themo Scientific in USA. Thiol end-functionalized peptide nucleic acid (thiolPNA, [38]) and terminal amino functioned SAF-93 with twenty thymine bases as the spacer were synthesized by Shanghai Sangon Biotechnology Co. in China. The terminal amino functioned anti-ricin aptamer (NH_2-$(CH_2)_6$-5′-(T_{20})-CGTAGGTTCGGGGCGGAGTGGTCCGGAAGGTGGCGTGG-3′) which was used as a control, was also synthesized by Shanghai Sangon Biotechnology Co. in China [26]. ThioPEG were purchased from Prochimia Surfaces in Poland. Cys-protein G (Catalog #: 1002-04) was obtained from Shanghai PrimeGene Bio-Tech Co. in China. Expandable graphitic flake (code no 50870) were purchased from Fluka. Other reagents were obtained from Sigma-Aldrich with analytical grade or higher.

2.2. Treatment of PrP^{C} and PrP^{Sc}

The purity of purchased prion protein was determined by SDS-PAGE as >95%. The protein was stored at −20 °C. Before each experiment, the protein was centrifuged (20,000 × *g*) for 4 °C to remove pre-existing aggregates. The transformation from PrP^{C} to

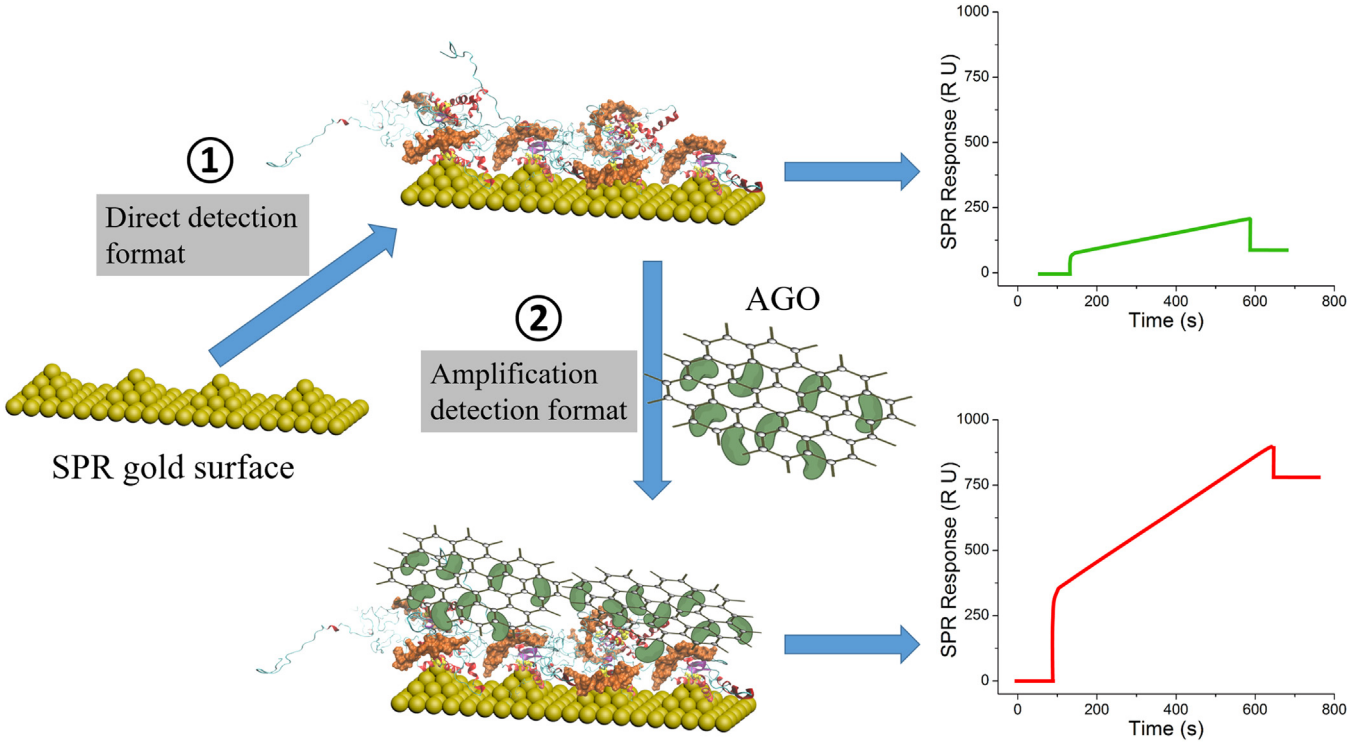

Fig. 1. Schematic representation of the SPR sandwich detection assay.

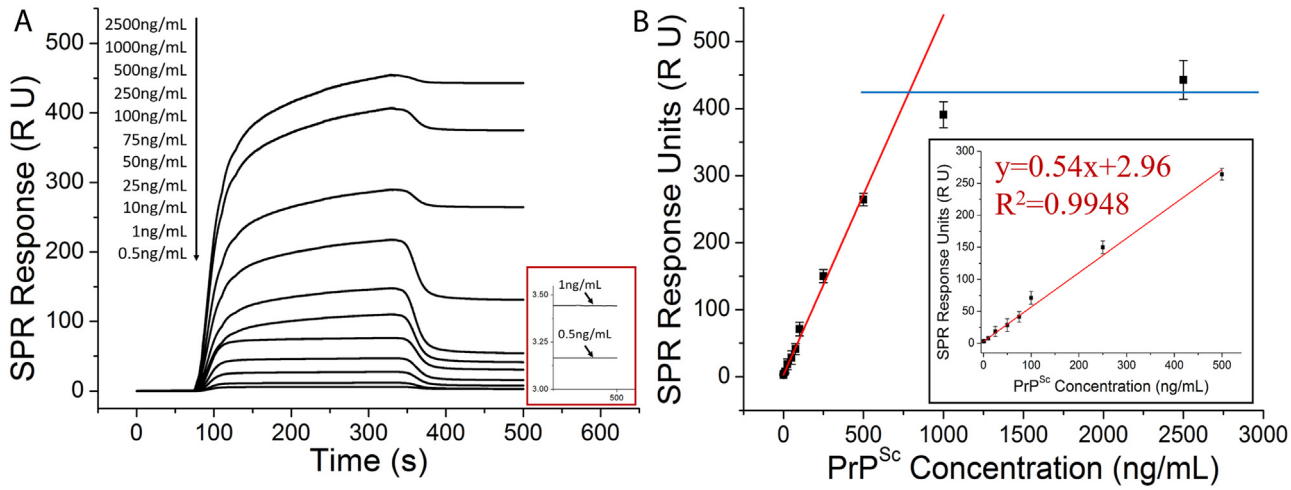

Fig. 2. (A) SPR sensorgram and (B) calibration curve of SPR direct detection of PrP^{Sc} utilizing bare gold film.

PrP^{Sc} was induced by incubation of PrP^{C} in sodium acetate-acetic acid buffer (pH 4.0).

The standard procedure to digest PrP^{C} and PrP^{Sc} samples consists of treating samples with proteinase K (PK, 50 μg/mL) for 60 min with shaking at 37 °C. The digestion was stopped with Laemmli electrophoresis buffer.

2.3. Synthesis of AGO conjugates

The carboxylic acid functioned graphite oxide (GO-COOH) was synthesized using the procedure and chemicals reported by Liu et al. [39].

Then EDC (75 mM) and NHS (15 mM) were added into the synthesized GO-COOH solution and the mixture was bath sonicated for 30 min. After that, the aptamer (10 μg, diluted in 200 μL PBS) was added and the mixture was bath-sonicated for another 10 min, followed by stirring for 12 h in 4 °C. The final product, AGO, was collected by centrifugation in PBS buffer.

The anti-ricin aptamer functioned GO sheets were synthesized in the same way, and were named as A_1GO.

2.4. Instruments and measurements

The biosensor system called BI-2000 along with the gold films (50 nm thick) was supplied by Biosensing Inc. (Arizona, USA). The gold film was mounted on a SPR prism with the matching oil. Then PrP^{Sc} samples with different concentrations in PBS buffer were successively injected onto the bare gold film. Then the AGO conjugates solution was injected into the cuvette to enhance the detection signals. To investigate the specificity and selectivity of the detection assay, mixture solutions of PrP^{Sc} and six other regents (3-mercaptopropionic acid (MPA), thioPEG, thioPNA, Cys-protein G, albumin from bovine serumin (BSA), and PrP^{C}) in different concentration proportions were introduced. Besides, the PK digested PrP^{Sc}, PrP^{C} and PrP^{C}/PrP^{Sc} mixture samples were also detected by the AGO enhanced SPR detection assay described here. The corresponding SPR signals were obtained in three repeated experiments independently.

An Agilent 5500 Controller combined with a 50 μm by 50 μm Agilent multipurpose AFM scanner was used to obtain high-resolution AFM imgaes. All the images were obtained in air at room temperature. Before the AFM imaging of the gold sensing surfaces after the detection processes, we dried the surfaces gently with nitrogen gas flow. For the AFM imaging of the GO and AGO sheets on mica surface, we firstly dropped the sample solution on freshly cleaved mica surface, and then dried the surface gently with nitrogen gas flow. Silicon cantilevers tip with spring constant of around 0.1 N/m were used for experiments. The images were acquired by using Agilent magnetic AC (MAC) mode AFM with a magnetically coated cantilever. The obtained AFM images were processed by WSxM software.

3. Results and discussion

3.1. Direct detection of PrP^{Sc}

For the direct detection format, after SPR baseline being kept constant caused by the chip surface being rinsed with PBS buffer, a series of PrP^{Sc} solutions with different concentrations were separately injected into the SPR cell, followed by being rinsed with PBS. Fig. 2A shows the representative real-time sensorgram of SPR for detection of PrP^{Sc} with direct detection format. The SPR responses gradually increase with the PrP^{Sc} concentration increasing from 0.5 to 2500 ng/mL in Fig. 2A (from 3.16 RU to 442.86 RU). The sensing film surfaces after the detection of PrP^{Sc} with the concentrations of 0.5, 50, 100, 250, and 500 ng/mL are shown by topography AFM images in Fig. 3. The corresponding 3D AFM images were shown in Fig. S2. It can be seen from Figs. 3 and S2 that, vastly different degrees of molecule coverage were observed, with the lower concentration inducing a lesser degree of PrP^{Sc} binding. For the surface exposed to 0.5 ng/mL PrP^{Sc} sample, only individual particles were observed by AFM. From the corresponding cross-section files of these particles, the height values of these particles were ~0.8 nm, which were consistent to our previous results [32]. With the increase of PrP^{Sc} concentration, we may see that the PrP^{Sc} molecules assembled on the gold films, forming monolayers with different degrees of density (Figs. 3 and S2). The height of these layers ranged from ~1.00 nm to ~1.2 nm, indicating that these layers were formed by PrP^{Sc} oligomers as previously reported [32]. All these results indicate that the SPR responses are attributed to the binding of PrP^{Sc} molecules onto the bare gold film.

The detection signal exhibited a good linear relationship with the concentration from 0.5 to 500 ng/mL (Fig. 2B), and concentrations as low as 0.5 ng/mL can be readily measured. The linear regression equation was $y = 0.54x + 2.96$ ($R^2 = 0.9948$, x is the concentration of PrP^{Sc} (ng/mL) and y is the SPR signal (RU)). SPR gold surface was almost saturated when the concentration was 500 ng/mL (Fig. 3), implying less active site remained free for the binding of PrP^{Sc} molecules when the concentration increased. This explained why the signal increased slightly with the increasing of the concentration from 500 to 2500 ng/mL.

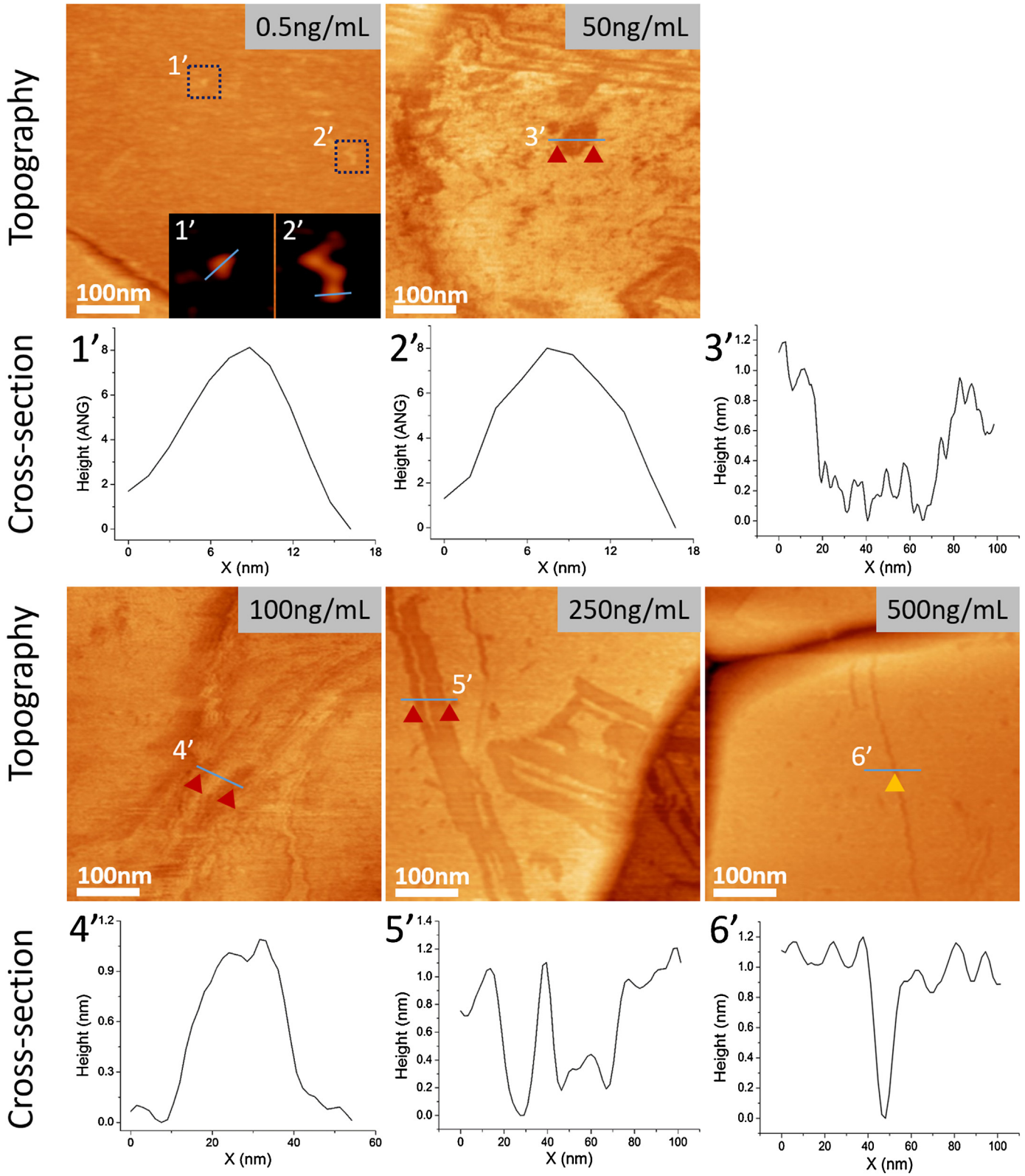

Fig. 3. The AFM topography images of the surface morphologies of the SPR gold surface after exposing to PrP^{Sc} solutions with different concentrations, and the corresponding cross-section profiles following the labeled lines. The corresponding 3D AFM images were in Fig. S2.

3.2. Characterization of GO and AGO

GO and AGO sheets were imaged on mica via AFM, and their corresponding thickness was collected. The results were shown in Fig. 4. From Fig. 4A and B, we may see that both GO and AGO were observed to be disk-like under AFM, indicating that the modification of aptamer on the GO sheets did not change their morphologies. The thickness of AGO was 12.21 ± 0.01 nm (Fig. 4C), which was much larger than the thickness of GO sheets (1.81 ± 0.01 nm, Fig. 4D). The increased thickness was attributed to

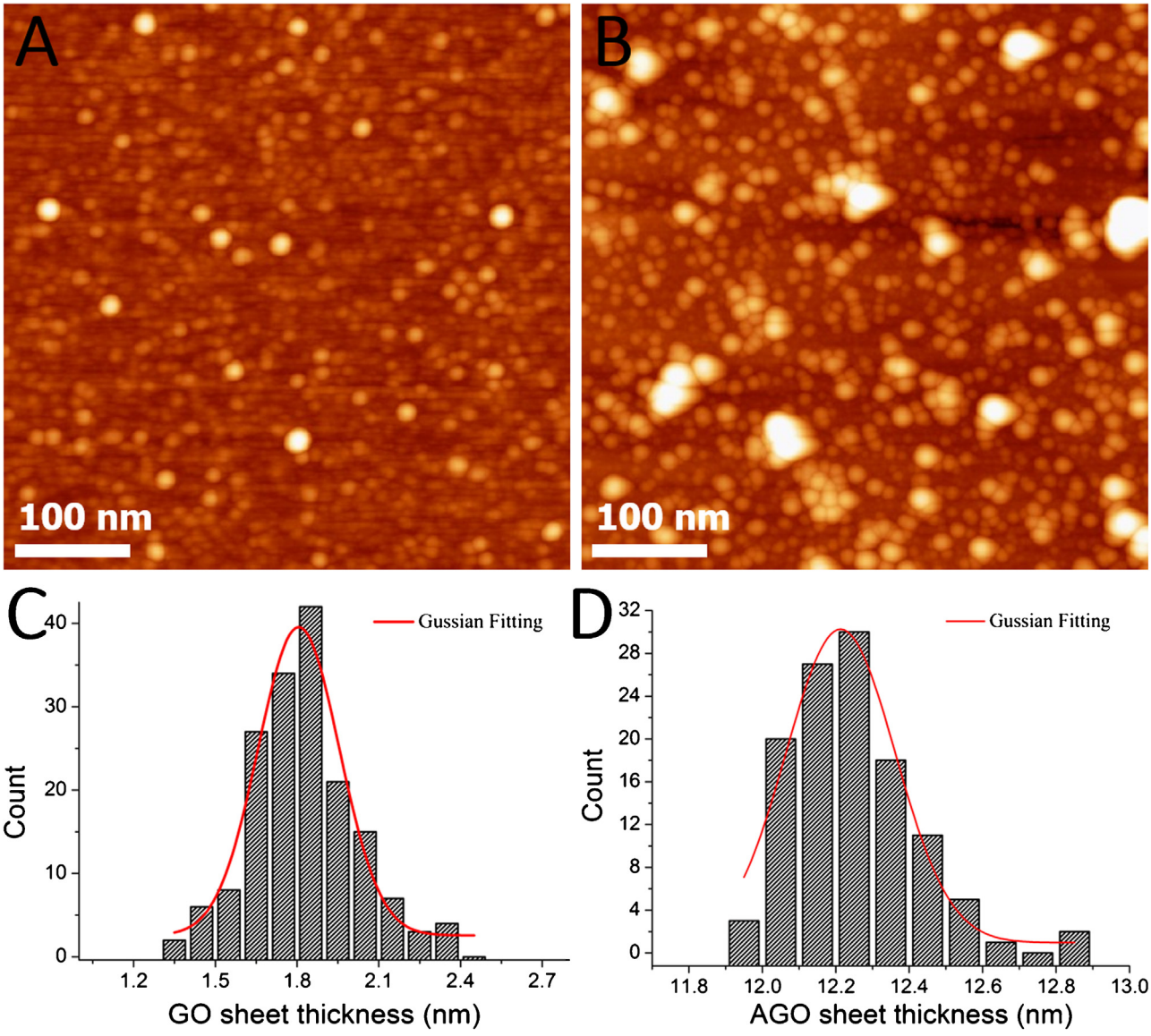

Fig. 4. AFM images of GO (A) and AGO (B). Thickness histogram of GO (C) and AGO (D) measured by AFM.

the modification of terminal amino functioned SAF-93 aptamer on GO sheets. Fig. S3 showed the UV–vis spectra of the GO and AGO. Compared with GO sheets, there was an additional absorption band of AGO at around 260 nm. As we know, 260 nm is the characteristic absorption band of nucleic acids (DNA [40] or RNA [41]). This result suggested the successful immobilization of aptamer on the GO sheets.

3.3. Amplification of SPR signals via AGO sheets

A series of PrP^{Sc} solutions with concentrations from 1 pg/mL to 250 ng/mL were firstly injected into the SPR cell, successively. Subsequently, when the SPR signal reached a plateau, the AGO solution was injected and the in situ SPR curve were shown in Fig. 5A. As shown in Fig. 5A, the SPR responses resulted from the binding of AGO increased gradually with increasing PrP^{Sc} concentration, enabling us to detect the trace PrP^{Sc}. The 1 pg/mL PrP^{Sc} induces SPR response of 20.94 RU. While the 250 ng/mL PrP^{Sc} results in a larger SPR response of 676.10 RU. A good linear relationship was obtained between SPR responses and the logarithm of PrP^{Sc} concentrations over a range of 0.001–1 ng/mL (Fig. 5B). The regression equation was $y = 547.12 + 178.35x$ ($R2 = 0.9904$, x is the logarithm of PrP^{Sc} concentration and y is the SPR signal). It may be obviously seen from Figs. 5B and 2B that the sensor response saturation for amplification detection format occurred at much lower PrP^{Sc} levels than direct detection format. The PrPSc concentrations as low as 0.001 ng/mL can be readily measured, which is around 500 lower than that by direct detection format (0.5 ng/mL).

Fig. 6A shows the representative AFM image of the surface morphology of the gold film after the AGO amplification detection assay for PrP^{Sc} solution with the concentration of 250 ng/mL. It can be seen from the *zoom-in* image and the corresponding cross-section profiles (Fig. 6B), the thickness of the AGO was ~12 nm, consistent to the results measured on mica surface (Fig. 4D). Fig. 6C is zoom-in image of the yellow squared area in Fig. 6B, evaluating the detailed morphology of the sensing surface. Both in the topography and corresponding 3D AFM images in Fig. 6C, we were able to visualize seven dots (pointed by arrows) on the GO surface, which were supposed to be aptamer-modified GO sheets. All these results indicated that, the AGO successfully attached onto the sensing surface via the specific interactions between AGO and PrP^{Sc} molecules, while the PrP^{Sc} molecules had already been captured via a cou-

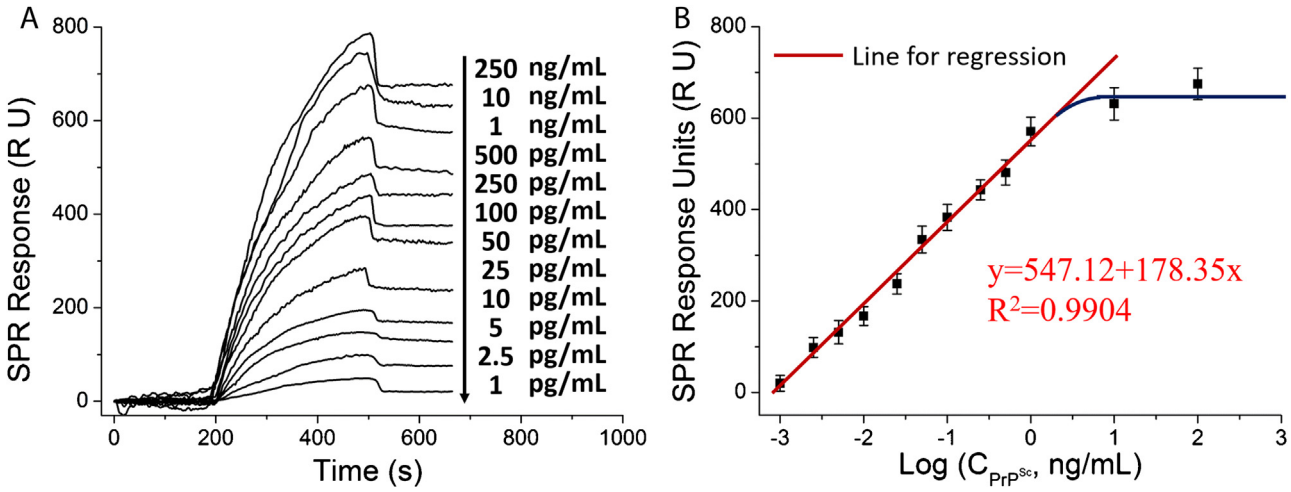

Fig. 5. (A) SPR sensorgram and (B) calibration curve of the enhanced SPR detection of PrP^{Sc} utilizing AGO.

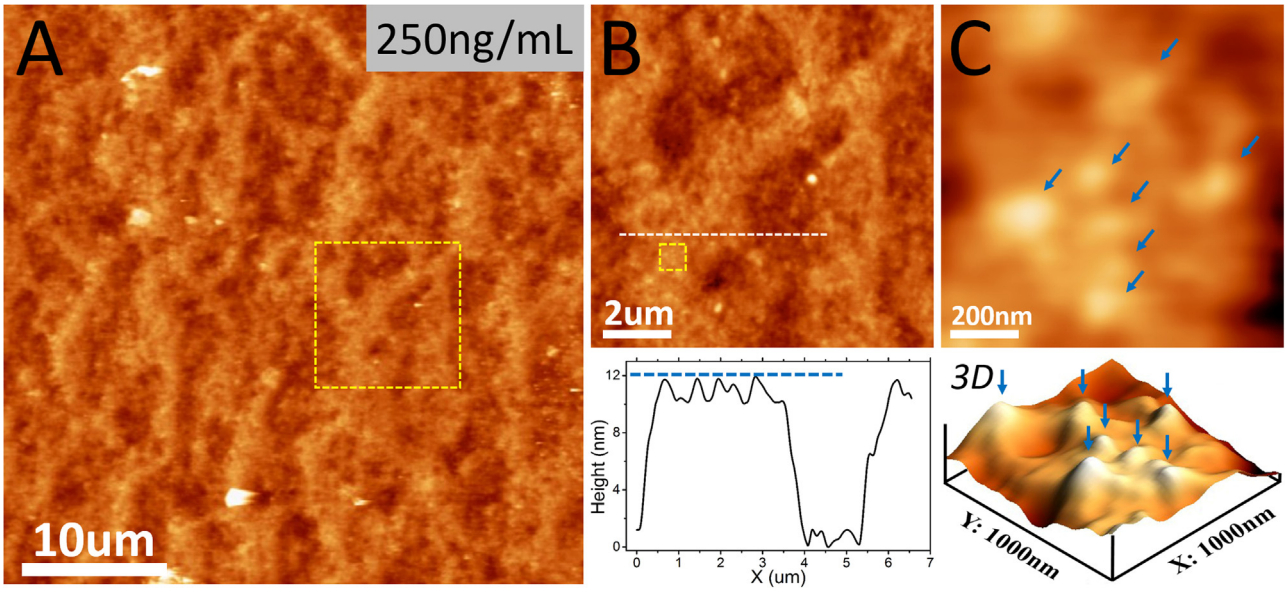

Fig. 6. (A) AFM image of the surface morphology of the gold film after the amplification assay when sample concentration is 250 ng/mL. (B) (Upper panel) the *zoom-in* image of the squared area in (A), (bottom panel) the cross-section profile following the dashed line in the AFM image. (C) The *zoom-in* topography and 3D AFM image of the squared area in (B). (For interpretation of the references to colour in the text, the reader is referred to the web version of this article.)

pling reaction between the intramolecular disulfide bond and gold atoms of the sensing surface. Besides, from the cross-section profiles in Fig. 6B, we may also observe the lower signals at around 1 nm (labeled by red dashed lines). These signals were supposed to be the height values of the exposed PrP^{Sc} molecules captured on the surface of sensing film. Again, because the SPR gold film was almost saturated of AGO when the concentration was 10 ng/mL, and less AGO could bind to the self-assembled PrP^{Sc} on the substrate due to steric hindrance, the signal increased slightly when the concentration was from 10 to 250 ng/mL. All these results indicate that the signal enhancement obtained here is attributed to the larger mass and higher refractive index of GO.

3.4. Specificity and selectivity

The sandwich SPR detection format described here required only one specific bio-probe, aptamer SAF-93, which was modified onto the GO sheets and interacted effectively with the captured PrP^{Sc} on the SPR sensing film. The specificity and selectivity of the sandwich detection assay were investigated. Pure PrP^{Sc}, PrP^{C}, Cys-protein G, and mixture solutions of PrP^{Sc} with other regents mentioned in Section 2.1, were detected by SPR. The SPR responds were further amplified with AGO. The corresponding direct and amplified SPR responds were collected in Fig. 7A. We may see from Fig. 7A that, all the samples induced appreciable but different direct SPR responds except of pure PrP^{C} sample. This is because that PrP^{C} have no affinity towards the bare gold film [32], and MPA, thiolPEG, PNA and Cys-protein G all have sulfhydryl groups and can assemble on the gold surface, leading to a high "non-specific" detection signals. But the SPR detection responds is conditioned by the refractive index change of the sensing film, which is intimately related to the molecular weight of the analytes. Here, the molecular weights of these four reagents are all lower than PrP^{Sc} [42–45]. When exposed to the PrP^{Sc} samples containing these four regents, part of the active sites of the bare gold film were occupied, leading a reduction of the binding amount of PrP^{Sc}. As a result, the direct SPR responds of these four mixtures (Cys-protein G/PrP^{Sc}, PNA/PrP^{Sc}, thiolPEG/PrP^{Sc} and MPA/PrP^{Sc}) were lower than that of pure PrP^{Sc}, BSA/PrP^{Sc} and PrP^{C}/PrP^{Sc}. This is because that BSA and PrP^{C} have no affinity towards the bare gold film. In spite of this, the

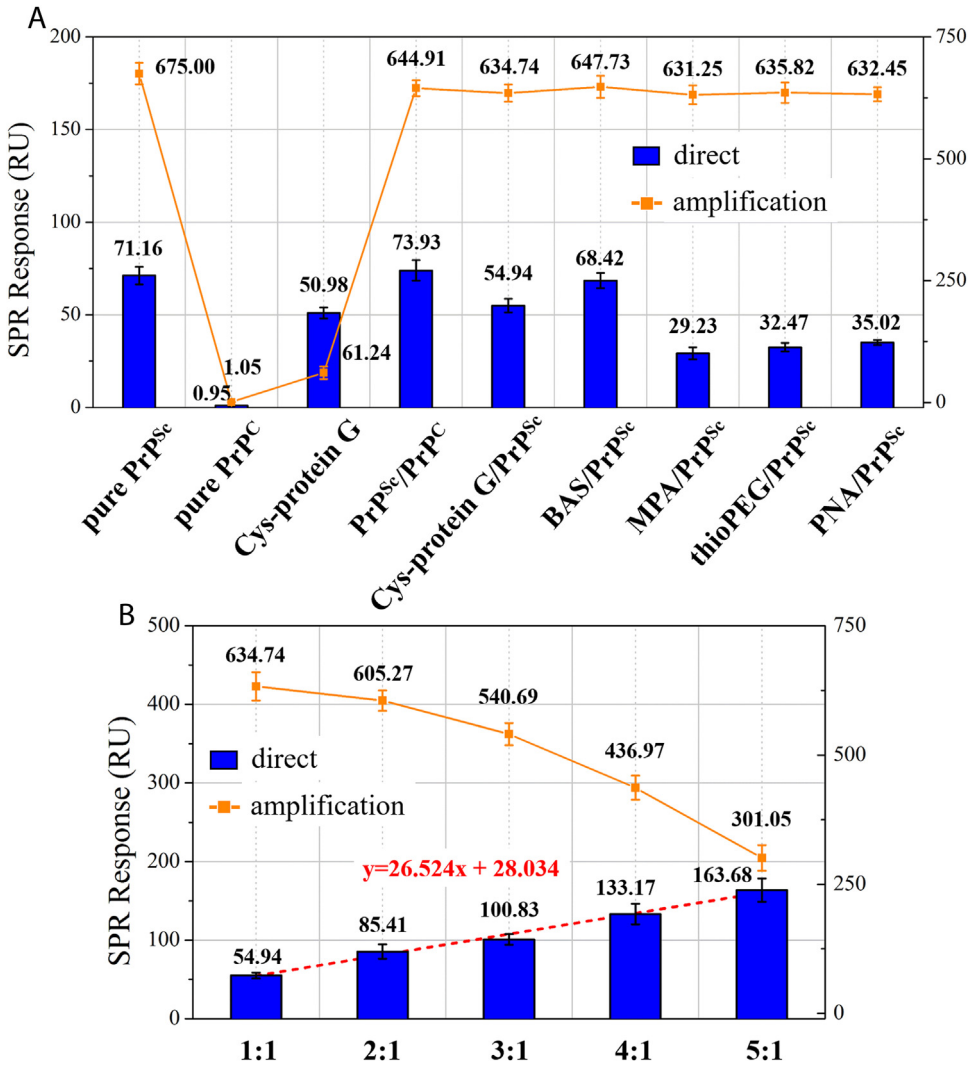

Fig. 7. The direct and enhanced SPR detection signals of the mixture solutions of PrP^{Sc} and other regents with the same concentration (A), and of the mixture solutions of PrP^{Sc} and Cys-protein G with different ratios in concentration (B).

enhanced signals still remained at high values (>630 RU) because of the existent PrP^{Sc} in these samples, which assembled onto the gold surface, providing binding sites for AGO. As comparison, pure Cys-protein G sample also induced an apparent SPR responds of 50.98 RU for the direct detection format, but the signal was not significantly improved by the amplified format (Δ = 10.26 RU) (Fig. 7A) because of the absence of PrP^{Sc}.

Fig. 7B is the direct and enhanced responds of the mixture solutions of PrP^{Sc} and Cys-protein G in different concentration proportions (concentration of PrP^{Sc} was fixed at 2.12 nM (50 ng/mL) while concentrations of Cys-protein G were 2.12, 4.24, 6.36, 8.48 and 10.6 nM). The direct signals showed a linear growth as the concentration of sulfhydryl groups increased gradually. But the enhanced signals caused by the specific binding of AGO to PrP^{Sc} showed a downward trend. This was because, with the growing proportion of Cys-protein G in the mixture solutions, more surface areas were occupied by Cys-protein G, causing that the amount of captured PrP^{Sc} on gold surface decreased, leading a reduction of the binding amount of the enhanced conjugates, AGO.

The specificity of AGO to the captured PrP^{Sc} and its non-specificity to the bare gold film were also investigated. The in situ SPR curves when AGO were injected into the SPR cell with and without PrP^{Sc}, along with the in situ SPR curve when A_1GO were injected into the SPR cell with PrP^{Sc}, were shown in Fig. S4. From Fig. S4 we may see that no SPR response was obtained for A_1Go. And it should be pointed out that the SPR response is around 3.76 RU for AGO without PrP^{Sc}. This is probably due to the non-specific adsorption of AGO onto the bare gold film. Even so, this response is much lower than that of AGO with PrP^{Sc} (569.62 RU).

PrP^{Sc} is partially resistant to proteolysis while PrP^{C} is protease sensitive. The PK treatment has been used conventionally in prion detection and discrimination, combining with the traditional detection assay, western blotting. However, this method is being questioned, considering that PK digests PrP^{Sc}, being responsible for the possibility of the occurrence of false negative data [46]. To investigate the specificity of the detection assay described here on the detection of PK digested samples, three samples were introduced and the corresponding direct and amplified SPR responds were collected in Fig. S5. We may see from Fig. S5 that, only for the samples consisting of PrP^{Sc} and without the treatment of PK digestion, the amplified SPR responds are at very high level (675.00 RU for PrP^{Sc} and 644.91 RU for PrP^{C}/PrP^{SC}), while the amplified SPR responds of the digested samples are much lower. Based on this, we may conclude that the detection assay described here is specific to the non-PK digested PrP^{Sc} samples, which is one of advantages of the present method to remove the need of the PK treatment during the detection process.

Table 1
Comparison with other reported methods.

Detection technique		type	time of analysis	working range (nM)	detection limit (nM)	reference
PMCA		PrP^{Sc}	9 h–44 h	N/A	~0.0033	[11]
ELISA		PrP^{Sc}	~5 h	N/A	0.08	[15]
micromechanical resonator arrays		PrP	~22 h	0.08–80	0.08	[14]
fluorescence correlation spectroscopy		PrP^{Sc}	1 h 3 min	N/A	0.13	[15]
real-time PCR		PrP^{Sc}	~20 h	5.38×10^{-9}–1.76×10^{-7}	3.85×10^{-9}	[17]
Quantum Dots	CdTe	rPrP	N/A	1–78	0.3	[47]
	CdSe/ZnS-Au NPs	PrP^{C}	~1 h	0.82×10^{-6}–3.30×10^{-6}	3.3×10^{-8}	[48]
	QDs-Magnetic NPs	PrP^{Res}	~2 h	0.8–306	0.086	[49]
Nanoparticles	aptamer-gold	rPrP	30 min	0.2–50	0.07	[50]
	bare gold	rPrP	40 min	0.1–50	~0.033	[51]
SPR	DNA aptamer	PrP^{C}	~1.5 h	50–100	4	[24]
	antibody	PrP^{C}	~1 h	2.12–21.2	1.34	[25]
AGO enhanced sandwich SPR assay		PrP^{Sc}	~30 min (direct)	0.021–21.21	below 0.021	This work
			~40 min (enhanced)	4.24×10^{-5}–4.24×10^{-2}	below 4.24×10^{-5}	This work

The detection limit, working range and time of analysis were comparable to these of the other reported methods (Table 1). It is easy to see that, the detection limit of AGO enhanced SPR detection assay described here is dramatically lower than that of the majority of other methods. Furthermore, the time required for the analysis of each sample using the present biosensor is only ~40 min, much faster than PMCA, ELISA, real-time PCR and other methods (Table 1). Therefore, our data indicate that AGO enhanced sandwich amplification can be used for fast detection of PrP. Although for the detection limit and detection time, the AGO enhanced assay have no advantage compared with these of Cdse/ZnS-Au NPs method, it has much wider detection range (from 0.21×10^{-2} to 4.24×10^{-5} nM) than the later.

4. Conclusions

We used bare gold film as SPR sensing film, for the purpose to avoid the interference from the traditional, complex and changeable probe-modified sensing surface. Aptamer-modified GO sheets were used for the amplification of detection signals, which were characterized by AFM and UV. A good linear relationship was obtained between SPR responses and the logarithm of PrP^{Sc} concentrations over a range of 0.001–1 ng/mL. The detection sensitivity for PrP^{Sc} was improved by ~156 orders of AGO compared with SPR direct detection format, indicating that AGO have excellent capability of amplifying SPR signals. Besides, morphological changes of the sensing film surfaces were investigated by high resolution AFM imaging, confirming the capture of PrP^{Sc} molecules and their further specific recognition by AGO. The excellent selectivity of the present biosensor was also confirmed by PrP^{C} and other regents as controls. The results reveal that this proposed approach could also be used to detect other analytes with intramolecular thiol groups by altering the corresponding aptamer in the AGO conjugates.

Acknowledgements

This work was supported by the National Natural Science Foundation of China (No. 61601227), Nature Science Foundation of Jiangsu Province (BK20160939), Natural Science Foundation of the Jiangsu Higher Education Institutions of China (16KJB180010), the Qing Lan Project and Priority Academic Program Development of Jiangsu Higher Education Institutions (PAPD).

Appendix A. Supplementary data

Supplementary data associated with this article can be found, in the online version, at http://dx.doi.org/10.1016/j.colsurfb.2017.05.058.

References

[1] Y. Wang, X.-Y. Qiao, C.-B. Zhao, X. Gao, Z.-W. Yao, L. Qi, C.-Z. Lu, Report on the first Chinese family with Gerstmann–Sträussler–Scheinker disease manifesting the codon 102 mutation in the prion protein gene, Neuropathology 26 (2006) 429–432.
[2] J. de Pedro-Cuesta, M. Glatzel, J. Almazán, K. Stoeck, V. Mellina, M. Puopolo, M. Pocchiari, I. Zerr, H.A. Kretszchmar, J.-P. Brandel, N. Delasnerie-Lauprêtre, A. Alpérovitch, C. Van Duijn, P. Sanchez-Juan, S. Collins, V. Lewis, G.H. Jansen, M.B. Coulthart, E. Gelpi, H. Budka, E. Mitrova, Human transmissible spongiform encephalopathies in eleven countries: diagnostic pattern across time, 1993–2002, BMC Public Health 6 (2006) 278.
[3] A. Ladogana, M. Puopolo, E.A. Croes, H. Budka, C. Jarius, S. Collins, G.M. Klug, T. Sutcliffe, A. Giulivi, A. Alperovitch, N. Delasnerie-Laupretre, J.-P. Brandel, S. Poser, H. Kretzschmar, I. Rietveld, E. Mitrova, J.P. de Cuesta, P. Martinez-Martin, M. Glatzel, A. Aguzzi, R. Knight, H. Ward, M. Pocchiari, C.M. van Duijn, R.G. Will, I. Zerr, Mortality from Creutzfeldt–Jakob disease and related disorders in Europe, Australia, and Canada, Neurology 64 (2005) 1586–1591.
[4] E. Biasini, J.A. Turnbaugh, U. Unterberger, D.A. Harris, Prion protein at the crossroads of physiology and disease, Trends Neurosci. 35 (2012) 92–103.
[5] W.-C. Yang, M.J. Schmerr, R. Jackman, W. Bodemer, E.S. Yeung, Capillary electrophoresis-based noncompetitive immunoassay for the prion protein using fluorescein-labeled protein a as a fluorescent probe, Anal. Chem. 77 (2005) 4489–4494.
[6] P.C. Klohn, L. Stoltze, E. Flechsig, M. Enari, C. Weissmann, A quantitative, highly sensitive cell-based infectivity assay for mouse scrapie prions, Proc. Natl. Acad. Sci. U. S. A. 100 (2003) 11666–11671.
[7] G.S. Jackson, L.L. Hosszu, A. Power, A.F. Hill, J. Kenney, H. Saibil, C.J. Craven, J.P. Waltho, A.R. Clarke, J. Collinge, Reversible conversion of monomeric human prion protein between native and fibrilogenic conformations, Science 283 (1999) 1935–1937.
[8] K.M. Pan, M. Baldwin, J. Nguyen, M. Gasset, A. Serban, D. Groth, I. Mehlhorn, Z. Huang, R.J. Fletterick, F.E. Cohen, Conversion of alpha-helices into beta-sheets features in the formation of the scrapie prion proteins, Proc. Natl. Acad. Sci. U. S. A. 90 (1993) 10962–10966.
[9] I.R. MacGregor, O. Drummond, Species differences in the blood content of the normal cellular isoform of prion protein PrP(c), measured by time-resolved fluoroimmunoassay, Vox Sang. 81 (2001) 236–240.
[10] B. Chen, R. Morales, M.A. Barria, C. Soto, Estimating prion concentration in fluids and tissues by quantitative PMCA, Nat. Methods 7 (2010) 519–520.
[11] G.P. Saborio, B. Permanne, C. Soto, Sensitive detection of pathological prion protein by cyclic amplification of protein misfolding, Nature 411 (2001) 810–813.
[12] H. Englund, D. Sehlin, A.-S. Johansson, L.N.G. Nilsson, P. Gellerfors, S. Paulie, L. Lannfelt, F.E. Pettersson, Sensitive ELISA detection of amyloid-β protofibrils in biological samples, J. Neurochem. 103 (2007) 334–345.
[13] M. Varshney, P.S. Waggoner, R.A. Montagna, H.G. Craighead, Prion protein detection in serum using micromechanical resonator arrays, Talanta 80 (2009) 593–599.
[14] M. Varshney, P.S. Waggoner, C.P. Tan, K. Aubin, R.A. Montagna, H.G. Craighead, Prion protein detection using nanomechanical resonator arrays and secondary mass labeling, Anal. Chem. 80 (2008) 2141–2148.
[15] F. Fujii, M. Horiuchi, M. Ueno, H. Sakata, I. Nagao, M. Tamura, M. Kinjo, Detection of prion protein immune complex for bovine spongiform encephalopathy diagnosis using fluorescence correlation spectroscopy and fluorescence cross-correlation spectroscopy, Anal. Biochem. 370 (2007) 131–141.
[16] B.M. Coleman, R.M. Nisbet, S. Han, R. Cappai, D.M. Hatters, A.F. Hill, Conformational detection of prion protein with biarsenical labeling and FlAsH fluorescence, Biochem. Biophys. Res. Commun. 380 (2009) 564–568.

[17] T. Reuter, B.H. Gilroyed, T.W. Alexander, G. Mitchell, A. Balachandran, S. Czub, T.A. McAllister, Prion protein detection via direct immuno-quantitative real-time PCR, J. Microbiol. Methods 78 (2009) 307–311.
[18] X.D. Hoa, A.G. Kirk, M. Tabrizian, Towards integrated and sensitive surface plasmon resonance biosensors: a review of recent progress, Biosens. Bioelectron. 23 (2007) 151–160.
[19] B. Liedberg, C. Nylander, I. Lunström, Surface plasmon resonance for gas detection and biosensing, Sens. Actuators 4 (1983) 299–304.
[20] C. Situ, M.H. Mooney, C.T. Elliott, J. Buijs, Advances in surface plasmon resonance biosensor technology towards high-throughput, food-safety analysis, TrAC Trends Anal. Chem. 29 (2010) 1305–1315.
[21] K.S. Lee, M. Lee, K.M. Byun, I.S. Lee, Surface plasmon resonance biosensing based on target-responsive mobility switch of magnetic nanoparticles under magnetic fields, J. Mater. Chem. 21 (2011) 5156–5162.
[22] A. Liang, Q. Liu, G. Wen, Z. Jiang, The surface-plasmon-resonance effect of nanogold/silver and its analytical applications, TrAC Trends Anal. Chem. 37 (2012) 32–47.
[23] J. Wang, A. Munir, Z. Zhu, H.S. Zhou, Magnetic nanoparticle enhanced surface plasmon resonance sensing and its application for the ultrasensitive detection of magnetic nanoparticle-enriched small molecules, Anal. Chem. 82 (2010) 6782–6789.
[24] A. Miodek, A. Poturnayová, M. Snejdárková, T. Hianik, H. Korri-Youssoufi, Binding kinetics of human cellular prion detection by DNA aptamers immobilized on a conducting polypyrrole, Anal. Bioanal. Chem. 405 (2013) 2505–2514.
[25] W. Jiayu, W. Xiong, L. Jiping, L. Wensen, X. Ming, L. Linna, X. Jing, W. Haiying, G. Hongwei, A rapid method for detection of PrP by surface plasmon resonance (SPR), Arch. Virol. 154 (2009) 1901–1908.
[26] B. Wang, Z. Lou, B. Park, Y. Kwon, H. Zhang, B. Xu, Surface conformations of an anti-ricin aptamer and its affinity for ricin determined by atomic force microscopy and surface plasmon resonance, Phys. Chem. Chem. Phys. PCCP 17 (2014) 307–314.
[27] Y. Li, H. Qi, J. Yang, C. Zhang, Detection of DNA immobilized on bare gold electrodes and gold nanoparticle-modified electrodes via electrogenerated chemiluminescence using a ruthenium complex as a tag, Microchim. Acta 164 (2009) 69.
[28] C. Garnier, L. Lesven, G. Billon, A. Magnier, Ø. Mikkelsen, I. Pižeta, Voltammetric procedure for trace metal analysis in polluted natural waters using homemade bare gold-disk microelectrodes, Anal. Bioanal. Chem. 386 (2006) 313–323.
[29] A. Thakur, G. Qiu, S.-P. Ng, J. Guan, J. Yue, Y. Lee, C.-M.L. Wu, Direct detection of two different tumor-derived extracellular vesicles by SAM-AuNIs LSPR biosensor, Biosens. Bioelectron. 94 (2017) 400–407.
[30] S. Li, M. Yang, W. Zhou, T.G. Johnston, R. Wang, J. Zhu, Dextran hydrogel coated surface plasmon resonance imaging (SPRi) sensor for sensitive and label-free detection of small molecule drugs, Appl. Surf. Sci. 355 (2015) 570–576.
[31] Z. Yue, W. Ye, W. Zhang, W. Li, G. Liu, C. Wang, Silver nanoparticle arrays enhanced spectral surface plasmon resonance optical sensor, Micro Nano Lett. 9 (2014) 585–587.
[32] Z. Lou, B. Wang, C. Guo, K. Wang, H. Zhang, B. Xu, Molecular-level insights of early-stage prion protein aggregation on mica and gold surface determined by AFM imaging and molecular simulation, Colloids Surf. B: Biointerfaces 135 (2015) 371–378.
[33] B. Wang, C. Guo, Z. Lou, B. Xu, Following the aggregation of human prion protein on Au(111) surface in real-time, Chem. Commun. 51 (2015) 2088–2090.
[34] A. Vallee, V. Humblot, C.-M. Pradier, Peptide interactions with metal and oxide surfaces, Acc. Chem. Res. 43 (2010) 1297–1306.
[35] S.Z. Nergiz, J.M. Slocik, R.R. Naik, S. Singamaneni, Surface defect sites facilitate fibrillation: an insight into adsorption of gold-binding peptides on Au(111), Phys. Chem. Chem. Phys. 15 (2013) 11629–11633.
[36] A. Rhie, L. Kirby, N. Sayer, R. Wellesley, P. Disterer, I. Sylvester, A. Gill, J. Hope, W. James, A. Tahiri-Alaoui, Characterization of 2′-fluoro-RNA aptamers that bind preferentially to disease-associated conformations of prion protein and inhibit conversion, J. Biol. Chem. 278 (2003) 39697–39705.
[37] N.M. Sayer, M. Cubin, A. Rhie, M. Bullock, A. Tahiri-Alaoui, W. James, Structural determinants of conformationally selective, prion-binding aptamers, J. Biol. Chem. 279 (2004) 13102–13109.
[38] X. Su, H.F. Teh, K.M.M. Aung, Y. Zong, Z. Gao, Femtomol SPR detection of DNA-PNA hybridization with the assistance of DNA-guided polyaniline deposition, Biosens. Bioelectron. 23 (2008) 1715–1720.
[39] Z. Liu, J.T. Robinson, X. Sun, H. Dai, PEGylated nanographene oxide for delivery of water-insoluble cancer drugs, J. Am. Chem. Soc. 130 (10876) (2008).
[40] C. Zimmer, G. Luck, H. Venner, J. Fric, Studies on the conformation of protonated DNA, Biopolymers 6 (1968) 563–574.
[41] A. Bürger, C. Wagner, C. Viedt, B. Reis, F. Hug, G.M. Hänsch, Fibronectin synthesis by human tubular epithelial cells in culture: effects of PDGF and TGF-β on synthesis and splicing, Kidney Int. 54 (1998) 407–415.
[42] S. Dong, J. Li, Self-assembled monolayers of thiols on gold electrodes for bioelectrochemistry and biosensors, Bioelectrochem. Bioenerg. 42 (1997) 7–13.
[43] A.P. Le Brun, S.A. Holt, D.S.H. Shah, C.F. Majkrzak, J.H. Lakey, The structural orientation of antibody layers bound to engineered biosensor surfaces, Biomaterials 32 (2011) 3303–3311.
[44] S. Ghosh, R. Mukhopadhyay, An atomic force microscopy investigation on self-assembled peptide nucleic acid structures on gold(111) surface, J. Colloid Interface Sci. 360 (2011) 52–60.
[45] J.M. Lee, H.K. Park, Y. Jung, J.K. Kim, S.O. Jung, B.H. Chung, Direct immobilization of protein G variants with various numbers of cysteine residues on a gold surface, Anal. Chem. 79 (2007) 2680–2687.
[46] M.A. Pastrana, G. Sajnani, B. Onisko, J. Castilla, R. Morales, C. Soto, J.R. Requena, Isolation and characterization of a proteinase K-sensitive PrPSc fraction, Biochemistry (Moscow) 45 (2006) 15710–15717.
[47] L. Liang, Y. Long, H. Zhang, Q. Wang, X. Huang, R. Zhu, P. Teng, X. Wang, H. Zheng, Visual detection of prion protein based on color complementarity principle, Biosens. Bioelectron. 50 (2013) 14–18.
[48] P.P. Hu, L.Q. Chen, C. Liu, S.J. Zhen, S.J. Xiao, L. Peng, Y.F. Li, C.Z. Huang, Ultra-sensitive detection of prion protein with a long range resonance energy transfer strategy, Chem. Commun. 46 (2010) 8285–8287.
[49] S.J. Xiao, P.P. Hu, X.D. Wu, Y.L. Zou, L.Q. Chen, L. Peng, J. Ling, S.J. Zhen, L. Zhan, Y.F. Li, C.Z. Huang, Sensitive discrimination and detection of prion disease-associated isoform with a dual-aptamer strategy by developing a sandwich structure of magnetic microparticles and quantum dots, Anal. Chem. 82 (2010) 9736–9742.
[50] H.-J. Zhang, Y.-H. Lu, Y.-J. Long, Q.-L. Wang, X.-X. Huang, R. Zhu, X.-L. Wang, L.-P. Liang, P. Teng, H.-Z. Zheng, An aptamer-functionalized gold nanoparticle biosensor for the detection of prion protein, Anal. Methods 6 (2014) 2982–2987.
[51] H.-J. Zhang, H.-Z. Zheng, Y.-J. Long, G.-F. Xiao, L.-Y. Zhang, Q.-L. Wang, M. Gao, W.-J. Bai, Gold nanoparticles as a label-free probe for the detection of amyloidogenic protein, Talanta 89 (2012) 401–406.